

# Online Episodic Memory Visual Query Localization with Egocentric Streaming Object Memory

Zaira Manigrasso<sup>▲\*</sup> Matteo Dunnhofer<sup>▲\*</sup> Antonino Furnari<sup>▼\*</sup>  
 Moritz Nottebaum<sup>▲</sup> Antonio Finocchiaro<sup>▼</sup> Davide Marana<sup>▲</sup>  
 Giovanni Maria Farinella<sup>▼\*</sup> Christian Micheloni<sup>▲\*</sup>

<sup>▲</sup> Machine Learning and Perception Lab, University of Udine, Italy

<sup>▼</sup> Image Processing Laboratory, University of Catania, Italy

## Abstract

Episodic memory retrieval aims to enable wearable devices with the ability to recollect from past video observations objects or events that have been observed (e.g., “where did I last see my smartphone?”). Despite the clear relevance of the task for a wide range of assistive systems, current task formulations are based on the “offline” assumption that the full video history can be accessed when the user makes a query, which is unrealistic in real settings, where wearable devices are limited in power and storage capacity. We introduce the novel task of Online Episodic Memory Visual Queries Localization (OEM-VQL), in which models are required to work in an online fashion, observing video frames only once and relying on past computations to answer user queries. To tackle this challenging task, we propose ESOM - Egocentric Streaming Object Memory, a novel framework based on an object discovery module to detect potentially interesting objects, a visual object tracker to track their position through the video in an online fashion, and a memory module to store spatio-temporal object coordinates and image representations, which can be queried efficiently at any moment. Comparisons with different baselines and offline methods show that OEM-VQL is challenging and ESOM is a viable approach to tackle the task, with results outperforming offline methods (81.92 vs 55.89 success rate%) when oracular object discovery and tracking are considered. Our analysis also sheds light on the limited performance of object detection and tracking in egocentric vision, providing a principled benchmark based on the OEM-VQL downstream task to assess progress in these areas.

\* denotes equal contribution. \* denotes equal supervision. Correspondence can be sent to: [matteo.dunnhofer@uniud.it](mailto:matteo.dunnhofer@uniud.it)

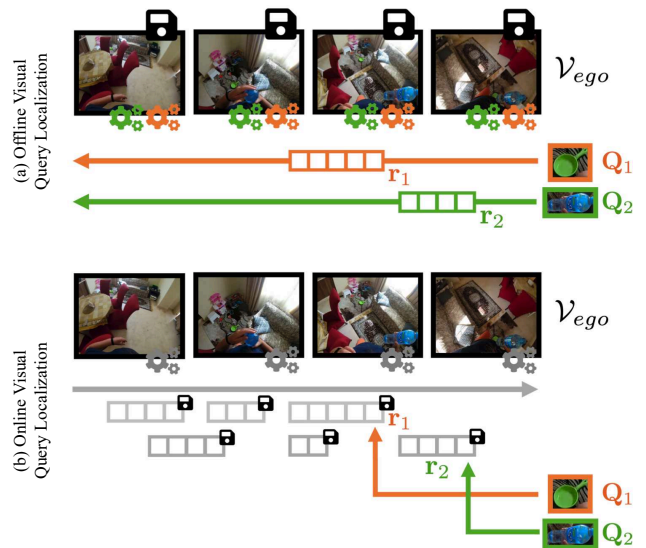


Figure 1. **Online visual query localization via object memorization and retrieval.** (a) Current approaches for visual query localization need to store (🔒) all the frames of a long egocentric video and process (⚙️) all of them to retrieve the response track ( $r_1$ ,  $r_2$ ) of each visual query ( $Q_1$ ,  $Q_2$ ). (b) We propose to process video frames only once (⚙️) and online, storing object representations (🔒) that may later be retrieved as response tracks ( $r_1$ ,  $r_2$ ) from visual queries ( $Q_1$ ,  $Q_2$ ). Our method replaces the need to store the entire video by creating an indexed data structure, which significantly reduces space requirements and speeds up query retrieval and localization.

## 1. Introduction

Day-to-day experiences often witness lapses in human memory. We may misplace objects within our homes (like searching for a passport), lose track of completed tasks (wondering if salt was added), forget the locations of past activities (where were tickets purchased?), and overlook the

status of objects in our surroundings (did I leave the garage door open?). Wearable devices observing human activities from an egocentric perspective have the potential to assist the recall of such episodic memories [43] in a wide range of scenarios by continuously keeping track of observed objects and events to alleviate cognitive overload and support the execution of daily tasks [33].

Since daily activities revolve around interactions with objects serving specific functions, such as tools and appliances, it is natural to design episodic memory retrieval systems around the ability to correctly recall the occurrence of specific object instances. Towards this direction, the Visual Queries (VQ) task has been introduced with the Episodic Memory (EM) benchmark of the Ego4D dataset [18]. The VQ task is formulated as follows: given an image patch of an object query and a long egocentric video, identify a *response track*, the precise spatio-temporal location of the last appearance of the object. The interest of the community in EM tasks has been fostered by the regular organization of international challenges, which recently spurred a number of technical solutions [6, 13, 25, 31, 46] and research works [22, 29, 34, 35, 47]. While demonstrating the feasibility of addressing the problem, all previously presented solutions operate in an offline manner. Specifically, given a visual query at frame  $t$ , they search within the same video, scanning it from current frame  $t$  backward up to the moment in which the object is found. This translates into algorithms that, for each new query object, necessitate storing and re-processing all the frames previously observed in the video stream. We argue that this approach is unfeasible in practical applications, especially considering a scenario in which an always-on wearable device processes several hours of video per day.<sup>2</sup> Additionally, processing different queries within the same video entails executing the algorithm several times. In essence, we argue that, despite the potential of current algorithms, an offline query object search is not practically applicable due to its significant computational and storage requirements.

In sharp contrast with this burdensome and offline scenario, we advocate that EM systems should be designed to work in an online fashion, with limited budgets for computation and storage reflecting the need to ultimately deploy the algorithms on wearable devices. Note that an online formulation of the episodic memory task brings several challenges, beyond the need for efficient systems. Specifically: 1) An online system has to identify objects which could be potentially queried in the future without any prior knowledge of their identity, in contrast with offline systems which begin the object search only *after* the object query is known; 2) The online system should be able to keep track of the different occurrences of a given object instance and form ap-

propriate response tracks in advance, in contrast with offline systems which initiate a separate search for each query; 3) The online system should be able to associate each of the potential response tracks with appropriate representations to enable future retrieval, in contrast with an offline system, which can directly compare the query patch with object candidates during the search process.

To address this challenge, in this paper, we propose ESOM - Egocentric Stream Object Memory, a novel architecture which processes egocentric video frames in an online fashion and keeps a low-dimensional, interpretable dynamic memory of all objects observed in past video (see Figure 1). This is achieved thanks to three main components: 1) an *object discovery* module which detects objects of interest in each input frame; 2) an online, long-term *visual object tracker* which takes over the discovered objects to track them in the video; 3) a dynamic *object memory* which stores past observations in the form of object tracks with associated visual representations. The object memory is maintained by an *object memory population* process which keeps the memory updated by running the object discovery and visual object tracker components at any frame, and can be queried by a *query retrieval and localization* process which allows to efficiently search within the memory when a new query is made and return the appropriate response track. Experiments on the established Ego4D episodic memory retrieval benchmark [18] show the effectiveness of the proposed ESOM architecture, which outperforms offline episodic memory retrieval methods when oracular object discovery and tracking components are considered, achieving a success rate of 81.92% vs 55.89% of the best offline method. We also show that results in real-world non-oracular settings are hindered by the limited performance of current detection and tracking algorithms, which suggests that further research efforts should be devoted to the development of these components, for which this work offers a principled benchmark grounded in the real-world downstream task of episodic memory retrieval.

The contributions of this work are as follows: 1) we are the first to introduce the novel task of online episodic memory retrieval; 2) we propose ESOM, a novel architecture based on continuous object discovery, tracking, memory update, and query, which is shown to be in principle competitive with offline methods; 3) we offer a benchmark based on Ego4D [18] of online episodic memory retrieval in general and object detection/tracking in egocentric vision.

## 2. Related Work

**Episodic Memory Visual Query Localization.** The problem of Visual Query Localization was initially formalized in [18], along with a baseline cascade solution that first searches for the query patch in every frame by means of a Siamese R-CNN [44], and then tracks it forward and back-

<sup>2</sup>For instance, a 24-hour 8-bit RGB video with 1408x1408 resolution captured at 20FPS [40] can take up to 3.43 TB of memory uncompressed.

ward in time with a short-term tracker [4] to obtain the temporal extent of the response track. Based on this formulation, a variety of methodologies explored different key factors such as balancing positive and negative examples [46], addressing domain and task biases [47], improving feature extractors [6, 31], and developing end-to-end single-stage frameworks [22] to improve performance and inference speed. Despite the progress in this area, all the aforementioned works are based on the offline assumption. In this paper, we formulate a novel Online Episodic Memory Visual Query Localization task (OEM-VQL) and offer a first approach and benchmark to tackle the task.

**Object Memory and Cognition.** Few previous works investigated the use of object memory to support cognition, manipulation, or video understanding in robotics [21], to support object permanence in manipulation tasks, and in egocentric vision [32], to mimic human spatial cognition keeping track of object instances in 3D when they are either in-sight or out-of-sight. Recent work [11, 17], in particular, explored the use of an object memory to address video understanding tasks such as generic question answering [11] and comprehension of object-based activities in long egocentric videos [17]. Differently from the aforementioned works, our method is the first to propose and tackle online episodic memory with an object memory, which raises significant challenges, such as dealing with egocentric video, accounting for *all* objects appearing in the scene, and accurately track object instances in the video.

**Online Processing in Egocentric Vision.** Some previous works tackled the design of algorithms and systems which to support online processing, a fundamental requirement for real-world applications on wearable devices [1, 7, 8, 14–16, 20, 37, 38, 41, 50], in contrast to a whole line of egocentric vision tasks such as action recognition [3, 5, 12] and temporal action detection [27, 49] which assume that the whole video is available at inference time. Episodic memory retrieval tasks, as initially formulated in [18] are based on the “offline” assumption. Limited amount of works considered an alternative online formulation which resembles an online setting [2], but a systematic investigation on the topic is still missing. We address the problem of online episodic memory retrieval targeting the VQL task. The developed system achieves online processing abilities by making use of visual object tracking and a compact queryable memory module to store past experiences.

### 3. Online Episodic Memory - Visual Queries

This paper addresses the challenge of locating an image patch of a query object instance within an online video stream that cannot be stored. We refer to this problem as the Online Episodic Memory - Visual Query Localization (OEM-VQL) task. More formally, given a streaming egocentric video  $\mathcal{V}_{ego} = \{\mathbf{F}_t\}$  of RGB frames  $\mathbf{F}_t$  indexed by

time  $t$ , and a query RGB image patch  $\mathbf{Q}$  containing the visual appearance of the query object, the goal is to return a response track:

$$\mathbf{r} = \{\mathbf{b}_s, \mathbf{b}_{s+1}, \dots, \mathbf{b}_{e-1}, \mathbf{b}_e\}, \quad (1)$$

i.e., an ordered sequence of bounding-boxes  $\mathbf{b}_j, s \leq j \leq e \leq t$  which determines the spatio-temporal position of the last appearance of the object in  $\mathcal{V}_{ego}$ .  $s$  and  $e$  are the starting and ending frames of the response track and each box  $\mathbf{b}_j$  corresponds to frame  $\mathbf{F}_j$ . As in [18], the goal is to find  $\mathbf{r}$  given  $\mathbf{Q}$ , however, critically, our formulation does not grant access to the complete video  $\mathcal{V}_{ego}$ . Rather, we allow methods to exploit just the visual information in  $\mathbf{F}_t$  plus compact object memories computed at previous frames  $\mathbf{F}_{\hat{t}}$  with  $\hat{t} < t$ . Figure 1 provides a visual illustration of our problem formulation in contrast to the one adopted in [18].

## 4. Egocentric Streaming Object Memory

To tackle OEM-VQL, we propose the Egocentric Streaming Object Memory (ESOM) architecture. ESOM is based on the object memory  $\mathcal{M}_{ego}$ , a dynamic data structure that memorizes relevant object instances appearing in  $\mathcal{V}_{ego}$ . The data structure is populated and queried through two processes: (i) the *object memory population* algorithm that builds such data structure online and continuously as the video  $\mathcal{V}_{ego}$  is being captured; (ii) the *query retrieval and localization* algorithm that retrieves the response track  $\mathbf{r}$  related to the visual query  $\mathbf{Q}$  from the constructed data structure, whenever needed by the camera wearer. The continuous interaction between these components allows to dynamically create, update, and query the memory of previously observed objects to support online episodic memory retrieval without the need of storing all the frames of  $\mathcal{V}_{ego}$  (see Figure 1).

### 4.1. Object Memory

The core component of the ESOM architecture is the object memory  $\mathcal{M}_{ego}$ , a dynamic data structure which maintains spatio-temporal information of object instances relevant to the camera-wearer and is updated at every frame  $\mathbf{F}_t$ .

**Representation.** We define the object memory as a set

$$\mathcal{M}_{ego} = \{\mathbf{O}_1, \dots, \mathbf{O}_i, \dots, \mathbf{O}_N\} \quad (2)$$

of compact, high-level representations  $\mathbf{O}_i$  of the spatio-temporal locations of objects in the frames  $\mathbf{F}_t$  of  $\mathcal{V}_{ego}$ . The indexes  $1 \leq i \leq N$  denote object instance unique IDs. While the representation of  $\mathbf{O}_i$  can be arbitrarily abstract, in practice, we set  $\mathbf{O}_i$  to be a list  $\mathbf{O}_i = \{\mathbf{o}_{i,t}\}$  of records temporally indexed by  $t$ , with each record having the following form

$$\mathbf{o}_{i,t} = [\mathbf{b}_{i,t}, \phi_{i,t}] \quad (3)$$

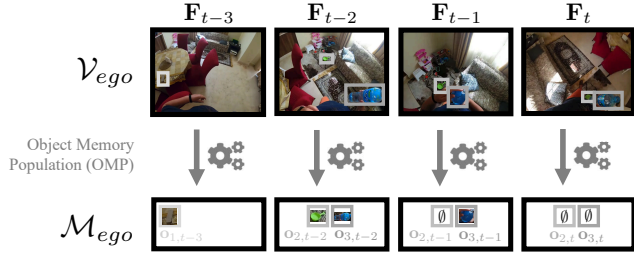


Figure 2. **From an egocentric video to a memory of objects.** ESOM injects the visual information in each frame  $F_t$  of a video  $V_{ego}$  into  $M_{ego}$ , an object memory represented as a dynamic list  $O_i$  of tuples  $\mathbf{o}_{i,t}$  composed of instance-based, frame-level bounding-boxes ( $\square$ ,  $\square$ ), and relative representations ( $\begin{smallmatrix} \text{img} \\ \text{img} \end{smallmatrix}$ ) which might be empty ( $\emptyset$ ) when considered not useful for retrieval.  $M_{ego}$  is built by an Object Memory Population (OMP) algorithm which processes ( $\text{gears}$ ) frames  $F_t$  online.

where  $\mathbf{b}_{i,t} = [b_{i,t}^x, b_{i,t}^y, b_{i,t}^w, b_{i,t}^h]$  denotes the object bounding-box, and  $\phi_{i,t}$  is a representation of the object’s appearance (e.g., in the form of RGB patches or extracted features). If  $\mathbf{o}_{i,t}$  is not visible in  $F_t$ , then  $\mathbf{o}_{i,t} = \emptyset$ . This formulation for the object memory provides an indexed, lightweight, compact, human-readable and easily queryable representation of objects observed in  $V_{ego}$  up to the current frame  $F_t$ . Figure 2 visualizes the representation of  $M_{ego}$  with respect to the visual information of  $V_{ego}$ .

**Interface.** Interaction with  $M_{ego}$  is achieved through two operations: `.read()`, and `.write()`. The `.read()` operation is used to access information on specific objects stored in  $M_{ego}$ . Following the object-oriented programming notation, we design `.read()` as an overloaded method that can take as input either an object ID  $i$  or a frame ID  $t$ .  $M_{ego}.\text{read}(i)$  returns the list of spatio-temporal localizations related to object instance  $O_i$ , whereas the  $M_{ego}.\text{read}(t)$  operation returns the spatial information of all objects  $O_i$  that are memorized at time  $t$ :

$$\{\mathbf{o}_{j,t}\} = M_{ego}.\text{read}(t), 1 \leq j \leq N \quad (4)$$

The `.write` operation allows to store new object instances or update existing ones. As before, this operation can be called with different input parameters. The syntax

$$M_{ego}.\text{write}([\mathbf{b}_{k,t}, \phi_{k,t}]) \quad (5)$$

stores with ID  $k$  (not yet present in  $M_{ego}$ ) a new object instance  $O_k$  by inserting the bounding-box  $\mathbf{b}_{k,t}$  and the representation  $\phi_{k,t}$ . The `write` operation can also be called as

$$M_{ego}.\text{write}([\mathbf{b}_{i,t}, \phi_{i,t}]) \quad (6)$$

to add bounding-box  $\mathbf{b}_{i,t}$  and visual representation  $\phi_{i,t}$  to object instance  $i$  at time  $t$  (i.e., we update the representation of  $O_i$ ). To create a consistent, yet compact, memory,

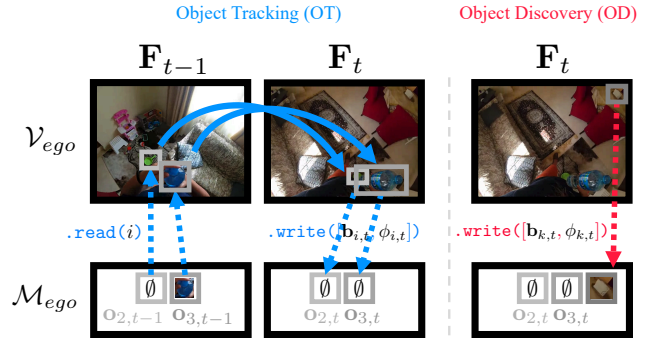


Figure 3. **Memory population by object tracking and discovery.** Between consecutive frames  $F_{t-1}$  and  $F_t$ , the **Object Tracking (OT)** module of the OMP algorithm reads the object representations  $\mathbf{o}_{i,t-1}$  (if stored in  $M_{ego}$ ), updates objects’ positions to  $\mathbf{b}_{i,t}$ , extracts representations  $\phi_{i,t}$ , and writes this information into  $M_{ego}$ . In parallel, new objects to store in  $M_{ego}$  are detected by the **Object Discovery (OD)** module in frame  $F_t$ . This provides bounding-boxes of relevant object instances  $\mathbf{b}_{k,t}$ , extracts representations  $\phi_{k,t}$  from them, and writes them to  $M_{ego}$ .

the `.write()` operation implements a filter to select which pieces of object information to be saved in  $M_{ego}$ . Information not useful to visual query retrieval should be excluded from  $M_{ego}$ . For instance,  $\phi_{i,t}$  might not contain sufficiently distinctive features for accurate instance recognition during retrieval. To avoid these situations, `.write([\mathbf{b}_{i,t}, \phi_{i,t}])` selectively saves only high-quality visual representations by replacing the previously memorized one, except for the first effective representation of the current tracklet. This selection is guided by a binary classification function that assigns a probability score to each  $\phi_{i,t}$ , indicating whether it is of sufficient quality for effective query retrieval (see Supp. material for details). In case of a negative decision, the visual representation is set to  $\phi_{i,t} = \emptyset$  and only the bounding-box is memorized. In this way, we retain the representation of the object at the moment of discovery, as well as two representations from the most recent response track that are as distant as possible from each other and considered effective by the classifier.

## 4.2. Object Memory Population (OMP)

The object memory  $M_{ego}$  is created and updated by a dedicated Object Memory Population (OMP) algorithm designed to process  $V_{ego}$  online. At each step  $t$ , this algorithm receives as input the latest available frame  $F_t$  and updates the object memory by executing an Object Tracking (OT) module and an Object Discovery (OD) module. A schematic visualization of the two modules within the OMP algorithm is given in Figure 3.

**Object Tracking Module.** The OT module is responsible for updating the localization of objects stored in  $M_{ego}$  at previous time steps, maintaining their unique IDs. At each frame  $F_t$ , the OT module first retrieves all previ-



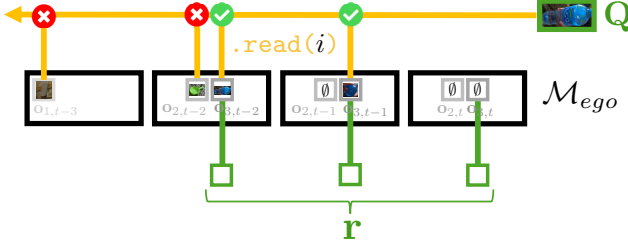


Figure 4. **Visual query localization by memory retrieval.** When the user provides a visual query  $Q$ , the Query Retrieval and Localization algorithm is triggered. This algorithm compares the representation of  $Q$  with the representations of each object  $O_i$  in  $M_{ego}$ . The sequence of contiguous bounding-boxes corresponding to the best-matched (✓) object is retained as the response track  $r$  for  $Q$ , while all other objects (✗) are discarded.

ously memorized objects  $O_i$  via  $M_{ego}.read(i)$ ,  $\forall i$ . The current bounding-box  $b_{i,t}$  is then computed by means of a visual object tracker [42, 48]. The visual tracker exploits the spatial and visual information stored in  $O_i$  to update the latest memorized bounding-box  $b_{i,\hat{t}}$ ,  $\hat{t} \leq t-1$  to  $b_{i,t}$ . Alongside each  $b_{i,t}$ , the tracker outputs confidence scores  $s_{i,t}$  and only bounding-boxes with  $s_{i,t} > \lambda_{ot}$  are retained. After filtering, the remaining bounding-boxes and their associated frame patches are written to memory as  $M_{ego}.write([b_{i,t}, \phi_{i,t}])$ . If no objects are stored in  $M_{ego}$ , i.e. when  $t = 0$  or until the new objects are inserted, the execution of the OT module is skipped. See the supplementary material for more details about the implementation of the OT module.

**Object Discovery Module.** The OD module is responsible for finding objects of interest in frame  $F_t$  which could be later queried by the user. OD is implemented as an object detector [45] which detects a set of  $B$  bounding-boxes  $b_{k,t}$  of objects in the frame, coupled with confidence scores  $s_{k,t}$ , with  $1 \leq k \leq B$ . After detecting the objects of interest, the OD module calls  $M_{ego}.read(t)$  to retrieve the bounding-boxes of all object instances already present in memory at time  $t$ . These are objects which may already have been tracked by the OT module at time  $t$  from object instances at time  $t-1$ . The detected boxes are first filtered based on  $s_{k,t} > \lambda_{od}$ . Those that do not have an IoU  $> \lambda_{iou}$  with any of the objects retrieved from the memory, are treated as localizations of new object instances. Their visual representations  $\phi_{k,t}$  are extracted exploiting  $b_{k,t}$ , and are then stored in memory by calling  $M_{ego}.write([b_{k,t}, \phi_{k,t}])$ , while the others are discarded. See the supplementary material for more details.

### 4.3. Query Retrieval and Localization (QRL)

The Query (QRL)Object Retrieval and Query Localization algorithm is responsible for retrieving the response track  $r$  of a visual query  $Q$  within the memory  $M_{ego}$ . This algo-

rithm takes  $Q$  as input and outputs a sequence of contiguous bounding-boxes  $b_{i,t}$  for the object instance  $O_i$  in  $M_{ego}$  that visually matches  $Q$ . The process begins by extracting feature representations  $\Phi(Q)$  using a feature extraction function  $\Phi(\cdot)$ . Such representation is then compared against the features  $\Phi(\phi_{i,t})$ ,  $\phi_{i,t} \neq \emptyset$  of each object  $O_i$  in  $M_{ego}$  that are read via  $M_{ego}.read(i)$  with a feature similarity function  $\Psi(\Phi(Q), \Phi(\phi_{i,t})) \in [0, 1]$ . The comparisons generate a sequence of  $[0, 1]$  scores corresponding to each stored visual representation  $\phi_{i,t}$ . For each object  $i$ , these values are averaged into a single score  $r_i$ . If the maximum score  $r_i$  exceeds the threshold  $\lambda_{ret}$ , the object  $O_i$  is considered a match for query  $Q$ . Once matched, the latest sequence of contiguous bounding-boxes from  $O_i$ 's spatio-temporal history is retrieved, returning it as the response track  $r$ . Note that this process relies exclusively on  $M_{ego}$ , and it does not require to access past frames from  $V_{ego}$ . Figure 4 provides an illustration of the process performed by QRL.

## 5. Experimental Settings

**Datasets.** To evaluate ESOM, we used the Ego4D Episodic Memory VQ2D benchmark [18, 42], including 433 hours of video from 54 scenarios, featuring over 22000 visual queries spanning 3000 object categories. At present time, this is the only publicly available annotated dataset for Visual Query Localization. To train components, we also use EgoTracks [42] an egocentric video dataset sourced from Ego4D and aligned to the episodic memory benchmark, and EgoObjects [51], a large-scale egocentric dataset for object detection.

**Implementation Details.** We tested different configurations of the proposed ESOM framework. In OMP, for the OT component, we used EgoSTARK [42], a STARK instance [48] fine-tuned on EgoTracks, as well as the MASA tracker [23]. To evaluate optimal tracking performance, we also considered ground-truth annotations from EgoTracks. We refer to these configurations as  $OT_{egostark}$ ,  $OT_{masa}$ ,  $OT_{oracle}$ .<sup>3</sup> For the OD module, we considered the off-the-shelf open-world detector GroundingDino [26], an instance of YOLOv10 [45] trained on curated versions of EgoTracks [42] and EgoObjects [51], and ground truth object detections from EgoTracks. These are denoted as  $OD_{gdino}$ ,  $OD_{yolo}$ ,  $OD_{oracle}$ .<sup>3</sup> In QRL, we implemented feature extraction  $\Phi(\cdot)$  and similarity  $\Psi(\cdot)$  using two configurations: Siam-RCNN with a classification head [44] or DINOv2 with cosine similarity [17, 30], referred to as  $QRL_{siamrcnn}$  and  $QRL_{dino}$ .<sup>3</sup> We obtained best results with  $OT_{egotracks}$ ,  $OD_{yolo}$  and  $QRL_{siamrcnn}$ , which identify the default configuration of ESOM where not otherwise specified.<sup>3</sup>

**Evaluation Protocol and Measures.** Each video clip  $V_{ego}$  in the evaluation dataset is fed to the OMP algorithm to con-

<sup>3</sup>See the supplementary material for more details.

Method	Approach	tAP $\uparrow$	tAP <sub>25</sub> $\uparrow$	stAP $\uparrow$	stAP <sub>25</sub> $\uparrow$	Succ $\uparrow$	Size $\downarrow$	Time $\downarrow$
1 SiamRCNN + KYS [18]	offline	0.12	0.20	0.04	0.12	39.80	12.1 GB	60.3 m
2 STARK [48]	offline	-	0.10	-	0.04	18.70	12.1 GB	60.3 m
3 SiamRCNN [44]	offline	-	0.22	-	0.15	43.24	12.1 GB	5.1 m
4 CocoFormer [47]	offline	-	0.27	-	0.20	48.37	12.1 GB	60.3 m
5 VQLoC [22]	offline	-	0.31	-	0.22	55.89	12.1 GB	5.1 m
6 ESOM - OD <sub>oracle</sub> - OT <sub>oracle</sub>	online	0.68	0.73	0.65	0.68	81.92	7.1 MB	0.51 s
7 ESOM - OD <sub>yolo</sub> - OT <sub>oracle</sub>	online	0.14	0.21	0.12	0.19	40.55	11.2 MB	0.36 s
8 ESOM - OD <sub>oracle</sub> - OT <sub>egostark</sub>	online	0.08	0.18	0.02	0.05	31.91	40.3 MB	0.49 s
9 ESOM - OD <sub>yolo</sub> - OT <sub>egostark</sub>	online	0.0001	0.0003	0.0005	0.002	4.02	209.3 MB	3.1 s

Table 1. **Comparison of ESOM for OEM-VQL versus offline VQL methods.** Using ESOM for tackling OEM-VQL offers significant savings in memory storage and enhances the efficiency of query localization. Overall performance depends largely on the performance the OT and OD modules, where tracking accuracy has the largest impact.

struct the object memory  $\mathcal{M}_{ego}$ . Each visual query  $\mathbf{Q}$  provided with the clip is then processed using the QRL algorithm, producing a response track  $\mathbf{r}$ , which we subsequently compare to the annotated ground-truth response track to compute query localization accuracy. We use the standard VQL evaluation metrics defined in [18]: tAP  $\uparrow$  measures temporal alignment with the ground-truth averaged over multiple IoU thresholds; tAP<sub>25</sub>  $\uparrow$ , computed at a 0.25 IoU threshold; stAP  $\uparrow$  assesses spatio-temporal precision, averaged across multiple thresholds; stAP<sub>25</sub>  $\uparrow$ , computed at a 0.25 spatio-temporal IoU threshold; Success (Succ  $\uparrow$ ) calculates the proportion of predictions with a minimum 0.05 spatio-temporal IoU with the ground-truth response track. In addition to these standard measures, we evaluate the efficiency of ESOM with storage size (Size  $\downarrow$ ) in multiples of bytes (MB, GB) needed to store information that enables query localization, and retrieval time (Time  $\downarrow$ ) in seconds (s) or minutes (m) that is required to localize a visual query.

## 6. Results

### 6.1. State-of-the-art Comparison

**OEM-VQL with ESOM vs offline VQL methods.** Table 1 compares different configurations of ESOM (rows 6-9) with state-of-the-art offline VQL methods (rows 1-5), highlighting significant advantages of ESOM in memory size and retrieval time. Offline methods require storing the entire video sequence, resulting in significant memory usage<sup>4</sup>. ESOM reduces memory needs by up to 1000 $\times$  when using oracular object discovery and tracking (row 6) and by 60 $\times$  when using non-oracular models (row 9). Additionally, ESOM’s retrieval time decreases from the several minutes required by offline methods (5 m at least - row 5) to just seconds (3.1 s at most - row 9), enabling faster response times. This efficiency is essential for real-world applications with memory constraints or requirement of real-time performance.

Due to the higher complexity of OEM-VQL, as com-

<sup>4</sup>We consider a fixed memory of 12.1 GB to store a 5-minutes clip as required in the EGO4D benchmark. Longer clips would take more space.

Method	tAP <sub>25</sub> $\uparrow$	stAP <sub>25</sub> $\uparrow$	Succ $\uparrow$	Size $\downarrow$	Time $\downarrow$
AMEGO [17]	0.0	0.0	0.67	241.7 MB	1.5 s
VideoAgent [11]	0.0002	0.001	3.03	1.2 GB	12.1 s
ESOM	<b>0.0003</b>	<b>0.002</b>	<b>4.02</b>	<b>209.3 MB</b>	3.1 s

Table 2. **ESOM’s memory representation enables more accurate online visual query localizations.** Comparison of ESOM with other methods to form object memories for OEM-VQL. (Best results are highlighted in **bold**).

pared to standard offline VQL, results of offline and online methods are not directly comparable. Despite this fact, when ESOM is equipped with optimal discovery and tracking (row 6), we achieve significant results that even outperform offline methods (81.92 Succ. vs the best offline Succ. of 55.89 - row 4). While oracular settings are not indicative of real-world performance, these results show the great potential of performing VQL online with the proposed ESOM architecture. Replacing the oracle object discovery model (OD<sub>oracle</sub>) with the state-of-the-art detector OD<sub>yolo</sub> reduces accuracy by roughly 50%, from 81.92 to 40.55 (rows 7 vs 6). Note that, despite object detections being imperfect, these results are still competitive with most offline methods (e.g., SiamRCNN and CocoFormer in rows 3-4 achieve similar (s)tAP metrics and slightly higher Succ.), while bringing the aforementioned benefits in size and time. Replacing oracular tracking with OT<sub>egostark</sub> while keeping the optimal object detector OD<sub>oracle</sub> brings a decline of 60% (row 8 vs 6). Despite the reduction in performance, this combination still outperforms the offline STARK baseline (row 2). The combined use of non-oracular components, OD<sub>yolo</sub> and OT<sub>egostark</sub>, leads to a drop in performance of about 95%, emphasizing the limitations of current state-of-the-art object detection and tracking algorithms, in particular when they are employed to tackle a challenging downstream task such as the proposed OEM-VQL. Note that, while previous studies highlighted the challenges of addressing object detection [51] and visual object tracking [9, 10, 42] in egocentric vision, the de-facto standard for evaluating such models

OMP Configuration	QRL	tAP <sub>25</sub> ↑	stAP <sub>25</sub> ↑	Succ ↑	Time ↓
OD OT					
OD <sub>oracle</sub> OT <sub>oracle</sub>	QRL <sub>siamrcnn</sub>	<b>0.73</b>	<b>0.68</b>	<b>81.92</b>	<b>0.51 s</b>
	QRL <sub>dino</sub>	0.64	0.57	76.00	0.56 s
OD <sub>yolo</sub> OT <sub>oracle</sub>	QRL <sub>siamrcnn</sub>	<b>0.21</b>	<b>0.19</b>	<b>40.55</b>	<b>0.36 s</b>
	QRL <sub>dino</sub>	0.20	0.12	35.53	0.4 s
OD <sub>oracle</sub> OT <sub>egostark</sub>	QRL <sub>siamrcnn</sub>	<b>0.18</b>	<b>0.05</b>	<b>31.91</b>	<b>0.49 s</b>
	QRL <sub>dino</sub>	<b>0.18</b>	<b>0.05</b>	30.68	0.54 s
OD <sub>yolo</sub> OT <sub>egostark</sub>	QRL <sub>siamrcnn</sub>	<b>0.0002</b>	<b>0.002</b>	<b>4.02</b>	<b>3.1 s</b>
	QRL <sub>dino</sub>	<b>0.0002</b>	<b>0.002</b>	3.79	3.4 s

Table 3. **Effect of the QRL algorithm on performance.** Performance of QRL methods across various OMP configurations. QRL<sub>siamrcnn</sub> consistently achieves the highest accuracy, making it the best-performing model for query retrieval in OEM-VQ. (Best results are highlighted in **bold**).

consists in assessing their performance in isolation [42, 51], which, we argue, may result in a distorted picture of the reliability of approaches for real-world applications. Besides setting a benchmark for the novel OEM-VQL task, our investigation also proposes a principled approach for evaluating object detection and tracking algorithms in egovision.

**ESOM versus other approaches based on object memory representations.** Table 2 compares ESOM with two baselines obtained combining our QRL method with object memory representations recently proposed for tasks other than Online Episodic Memory. AMEGO [17] is designed to tackle interaction-based egocentric video understanding tasks and focuses on objects that the camera wearer has interacted with by hand, whereas VideoAgent [11] tackles video question answering and focuses on generic objects. The results show that, while AMEGO offers competitive memory usage and query localization times, its overall performance is very limited. This is likely due to its focus on interacted objects, which may result in discarding important future object queries. VideoAgent’s accuracy is closer to ESOM’s. However, this comes at a cost of much higher memory usage and query retrieval time, which ESOM reduces by approximately six and four times respectively. This is due to the focus of VideoAgent on generic objects, while ESOM is optimized to target object queries.

## 6.2. Analysis of ESOM and Ablations

**Effect of QRL algorithm on performance.** Table 3 compares the performance of the QRL algorithm under the two considered implementations. QRL<sub>siamrcnn</sub> consistently performs best in matching a visual query with a memory of stored representations. Across all memory constructions produced by various OMP configurations, QRL<sub>siamrcnn</sub> demonstrates superior query localization scores, emphasizing its strength and adaptability for the OEM-VQ task.

**Filtering visual representations helps storage and query retrieval.** We assessed how the filtering operation performed by means of the binary classifier during the

OMP Configuration	$\phi_{i,t}$ filter	tAP <sub>25</sub> ↑	stAP <sub>25</sub> ↑	Succ ↑	Size ↓
OD OT					
OD <sub>oracle</sub> OT <sub>oracle</sub>	✓	<b>0.73</b>	<b>0.68</b>	<b>81.92</b>	<b>7.1 MB</b>
	✗	0.71	0.67	81.37	395 MB
OD <sub>yolo</sub> OT <sub>oracle</sub>	✓	<b>0.21</b>	<b>0.19</b>	<b>40.55</b>	<b>11.2 MB</b>
	✗	0.18	0.18	<b>40.55</b>	94.1 MB
OD <sub>oracle</sub> OT <sub>egostark</sub>	✓	<b>0.18</b>	<b>0.05</b>	<b>31.91</b>	<b>40.3 MB</b>
	✗	0.17	<b>0.05</b>	29.78	350.2 MB
OD <sub>yolo</sub> OT <sub>egostark</sub>	✓	0.0002	<b>0.002</b>	<b>4.02</b>	<b>209.3 MB</b>
	✗	<b>0.0003</b>	0.001	2.68	2.3 GB

Table 4. **Memorizing good visual representations improves storage and retrieval.** Keeping only good quality visual representation into the memory through filtering improves performance and reduces memory size. (Best results in **bold**).

.write() process affects memory size and the accuracy of QRL (Table 4). In the absence of the filtering operation, the memory is populated with the bounding boxes of all frames, along with the patches from the most recent response track, hence leading to an increased size. Downstream VLQ performance is generally improved by filtering, thanks to a more compact and uncluttered memory, with the added benefit of a decreased memory size.

**Effect of OD and OT modules.** Table 5 presents the performance of ESOM under different configurations of the OD and OT modules, reporting module-specific and VQL task performance metrics: AP ↑ and Rec ↑ for object detection<sup>5</sup>, HOTA ↑ and AssA ↑ for object tracking [28], and (s)tAP<sub>25</sub>, Succ., Size and Time for downstream OEM-VQL.

The OD module has a noticeable impact on performance, as weaker detectors might miss important queries and add objects into memory that are unlikely to be queried later. Notably, the open-world OD<sub>gdino</sub>, which is designed to detect a wide range of object instances, exhibits low recall and AP for annotated queries, leading to weak retrieval results even when used with oracular tracking OT<sub>oracle</sub>. In contrast, OD<sub>yolo</sub>, explicitly trained to target the queried objects enables effective memorization, resulting in more accurate QRL performance. Changes in the detector significantly affect memory size and processing time, with OD<sub>gdino</sub>, which detects a larger amount of objects, leading to a larger set of objects stored in memory. This expansion in memory size increases the time needed to localize a query.

OT modules have a more significant impact on performance. Indeed, changing the oracular tracker OT<sub>oracle</sub> with OT<sub>egostark</sub> while maintaining the oracular object discovery OD<sub>oracle</sub> brings Succ. down from 81.92 to 31.91. Interestingly, downstream performance seems to be inversely correlated with general tracking performance, with OT<sub>masa</sub> obtaining best HOTA ↑ scores (50.1 vs 21.7), but significantly smaller Succ. (9.38 vs 31.91), stAP<sub>25</sub> (0.01 vs 0.05) and tAP<sub>25</sub> (0.02 vs 0.18). Instead we observe correlation between VQL scores and association accuracy AssA, reveal-

<sup>5</sup>We merge all detections in a single “object” class.

OMP Config. OD	AP $\uparrow$	Rec $\uparrow$	OMP Config. OT	HOTA $\uparrow$	AssA $\uparrow$	tAP <sub>25</sub> $\uparrow$	stAP <sub>25</sub> $\uparrow$	Succ $\uparrow$	Size $\downarrow$	Time $\downarrow$
<i>OD<sub>oracle</sub></i>	100.0	100.0	<i>OT<sub>oracle</sub></i>	100.0	100.0	0.73	0.68	81.92	7.1 MB	0.51 s
			<i>OT<sub>masa</sub></i>	<b>50.1</b>	25.2	0.02	0.01	9.38	191.7 MB	7.2 s
			<i>OT<sub>egostark</sub></i>	21.7	<b>34.7</b>	<b>0.18</b>	<b>0.05</b>	<b>31.91</b>	<b>40.3 MB</b>	<b>0.49 s</b>
<i>OD<sub>yolo</sub></i>	13.6	30.7	<i>OT<sub>oracle</sub></i>	84.8	94.3	0.21	0.19	40.55	11.2 MB	0.36 s
			<i>OT<sub>masa</sub></i>	<b>6.6</b>	<b>11.6</b>	<b>0.001</b>	<b>0.001</b>	3.75	<b>46.7 MB</b>	<b>0.72 s</b>
			<i>OT<sub>egostark</sub></i>	6.1	<b>15.1</b>	0.0003	0.002	<b>4.02</b>	209.3 MB	3.1 s
<i>OD<sub>gdino</sub></i>	4.5	25.7	<i>OT<sub>oracle</sub></i>	87.5	94.3	0.15	0.12	33.33	14.7 MB	0.49 s
			<i>OT<sub>masa</sub></i>	3.6	10.5	0.0	0.0	0.70	<b>464.5 MB</b>	<b>2.5 s</b>
			<i>OT<sub>egostark</sub></i>	<b>5.7</b>	<b>15.1</b>	<b>0.0004</b>	0.0	<b>0.72</b>	2.9 GB	24.1 s

Table 5. **Effects of OD and OT modules on performance.** Different OD and OT model implementations determine different behaviors of the OMP algorithm, resulting in different memory representations. This, in turn leads to different QRL results. Performance of methods with oracular object tracking is reported in gray. (Best results are in bold).

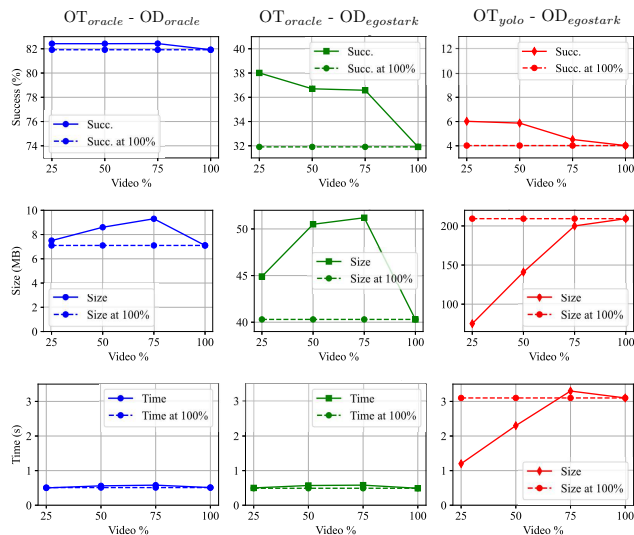


Figure 5. **ESOM scales well while increasing memory size.** Each row of plots shows how success score, storage space, and retrieval time change when performing QRL on memory built from progressively processed video segments. Results are shown for three different OMP configurations.

ing that ID association is important for accurate response track prediction. Results with *OD<sub>yolo</sub>* and *OD<sub>gdino</sub>* for object discovery are more nuanced, but reveal similar inconsistencies between tracking and downstream metrics. Being explicitly optimized for egovision, *OT<sub>egostark</sub>* has the best downstream performance.

#### Behavior of ESOM with different amounts of memory.

Figure 5 shows retrieval performance, storage space, and retrieval time as 25%, 50%, 75%, and 100% of videos are observed with different OMP configurations. QRL performance declines only slightly with video length and remains steady with oracular OD and OT, while minor drops occur with *OD<sub>oracle</sub>* and *OD<sub>egostark</sub>*, underscoring ESOM’s scalability. Storage and retrieval time generally increase over time; however, memory size remains stable with *OD<sub>oracle</sub>* since most objects appear within the first 25% of the video.

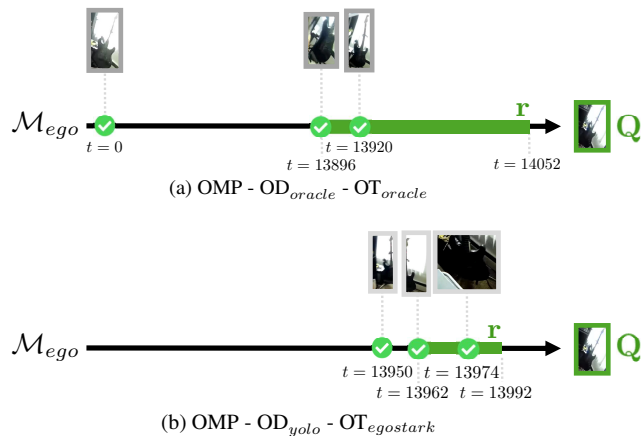


Figure 6. **Qualitative example.** Successful retrieval of query *Q* from  $\mathcal{M}_{ego}$  is shown using (a) the oracle OMP algorithm (*OD<sub>oracle</sub>* - *OT<sub>oracle</sub>*) and (b) the real-world OMP (*OD<sub>yolo</sub>* - *OT<sub>egostark</sub>*). The figure highlights the visual representations stored in  $\mathcal{M}_{ego}$  and matched during retrieval, their respective timestamps, and the duration of the response track *r*.

The *OD<sub>yolo</sub>* - *OT<sub>egostark</sub>* configuration significantly impacts storage and retrieval due to duplicate objects from weaker tracking.

**Qualitative Results.** Figure 6 shows a qualitative example of QRL retrieving and localizing a visual query within two memory representations.

## 7. Conclusions

We introduced the novel task of Online Episodic Memory - Visual Query Localization (OEM-VQL), where an object query must be localized in the past without access to the original video. To address this task, we proposed ESOM (Egocentric Stream Object Memory), a new online approach that memorizes only essential objects to support efficient visual query retrieval and localization. ESOM significantly reduces memory and computational demands, achieving up to a 1000 $\times$  reduction in memory usage and retrieval times from minutes to seconds. Experi-



ments on the Ego4D dataset show ESOM’s superior accuracy (81.92% with oracular models) over offline methods (55.89%), though real-world performance is still limited by current detection and tracking technology. Besides establishing a benchmark for OEM-VQL, we also contribute a principled evaluation, based on a real downstream task, for object detection and tracking algorithms for egovision applications.

**Acknowledgements.** This work was funded by European Union- NextGenerationEU under Project PRIN 2022 PNRR TEAM.

# Online Episodic Memory Visual Query Localization with Egocentric Streaming Object Memory

## Supplementary Material

This document reports implementation details on the proposed ESOM methodology, along with additional results and discussion. Specifically, Section A explains the ESOM architecture by providing details of the Object Memory representation (sub-section A.1), the Object Tracking (OT) module (sub-section A.2.2), on the Object Discovery (OD) module (Section A.2.2), and on the Query Retrieval and Localization (QRL) algorithm (sub-section A.3). Section B reports details on the implementation of the baselines methods on AMEGO [17] and VideoAgent [11]. Section C reports information on the evaluation dataset and Section D reports additional and qualitative results.

### A. Implementation Details of ESOM

#### A.1. Object Memory

**Memory representation.** We defined the object memory  $\mathcal{M}_{ego}$  as a set of high-level representations  $\mathbf{O}_i$  that capture the spatio-temporal locations of the objects in the frames  $\mathbf{F}_t$  of a video  $\mathcal{V}_{ego}$ . Each index  $1 \leq i \leq N$  corresponds to a unique object instance. The object representation  $\mathbf{O}_i$  is structured as a list of records, temporally indexed by  $t$ , where each record having the following form:  $\mathbf{o}_{i,t} = [\mathbf{b}_{i,t}, \phi_{i,t}]$ . Here  $\mathbf{b}_{i,t} = [b_{i,t}^x, b_{i,t}^y, b_{i,t}^w, b_{i,t}^h]$  denotes the object’s bounding box, and  $\phi_{i,t}$  represents the object’s visual representation at time  $t$  as the RGB patch outlined by the bounding-box  $\mathbf{b}_{i,t}$ . The design of  $\mathcal{M}_{ego}$  was driven by experimental results. Indeed, we evaluated various memory representations, focusing on four distinct forms of objects representation  $\mathbf{O}_i$ :

- MR1\* (design as reported in Section 4.1 of the main paper): for every object  $\mathbf{O}_i$ , the memory  $\mathcal{M}_{ego}$  retains the RGB patch ( $\phi_{i,t}$ ) and  $\mathbf{b}_{i,t}$  of the object at the moment of object discovery, as well as two RGB patches belonging to the most recent response track. These patches are chosen as the first and last valid patches identified by the classifier within the most recent sequence of bounding-boxes. For all other temporal locations not mentioned above, the memory  $\mathcal{M}_{ego}$  stores only the spatio-temporal information provided by  $\mathbf{b}_{i,t}$ .
- MR2: for every object  $\mathbf{O}_i$ , the memory  $\mathcal{M}_{ego}$  retains the RGB patch ( $\phi_{i,t}$ ) and  $\mathbf{b}_{i,t}$  of the object at the moment of object discovery, as well as all the RGB patches ( $\phi_{i,t}$ ) and bounding-boxes  $\mathbf{b}_{i,t}$  belonging to the most recent response track, considered useful by the classifier. For all other frames in temporal locations not mentioned, the memory  $\mathcal{M}_{ego}$  stores only the spatio-temporal infor-

mation provided by  $\mathbf{b}_{i,t}$ . This implementation was conducted to assess the impact of exploiting more object visual information for QRL.

- MR3: for every object  $\mathbf{O}_i$ , the memory  $\mathcal{M}_{ego}$  retains the RGB patch ( $\phi_{i,t}$ ) and  $\mathbf{b}_{i,t}$  of the object at the moment of object discovery. For all the other temporal locations, the memory  $\mathcal{M}_{ego}$  stores only the spatio-temporal information provided by  $\mathbf{b}_{i,t}$ . This implementation was conducted to assess the impact of exploiting less object visual information for QRL, thus to reduce the size and processing time of  $\mathcal{M}_{ego}$ .
- MR4: for every object  $\mathbf{O}_i$ , the memory  $\mathcal{M}_{ego}$  retains the RGB patch ( $\phi_{i,t}$ ) and  $\mathbf{b}_{i,t}$  of the object at the moment of object discovery as well as the RGB patches ( $\phi_{i,t}$ ) and  $\mathbf{b}_{i,t}$  in the first set of contiguous bounding-boxes (i.e., the beginning of each tracklet). For all the other temporal locations, the memory  $\mathcal{M}_{ego}$  stores only the spatio-temporal information provided by  $\mathbf{b}_{i,t}$ . This implementation was conducted to assess the impact of exploiting object visual information for QRL that refers to a better performance of the OT module.

The OEM-VQL performance of these memory configurations built by the Object Memory Population (OMP) algorithm and processed by the Query Retrieval and Localization (QRL) algorithm are reported in Table 6. As can be noticed, the proposed memory representation (MR1\*) offers the best balance between QRL accuracy and memory size and retrieval time.

**Visual representation filter.** To create a consistent yet compact memory, the `.write()` operation incorporates a filtering mechanism to determine which pieces of object information are stored in  $\mathcal{M}_{ego}$ . This filtering process relies on a binary classification function that assigns a probability score to each visual representation  $\phi_{i,t}$ , assessing its quality for effective query retrieval. The classification model was implemented using a deep neural network consisting of a ResNet18 [19] feature extractor and a linear layer, which served as the representation filter. This model was fine-tuned on a dataset of 17071 visual representations extracted from 250 uniformly sampled clips from the training set of the Ego4D Episodic Memory VQ2D-EgoTracks benchmark [18, 42]. Specifically, the training set included 8534 visual representations labeled as 0 (i.e., not suitable for QRL) and 5153 representations labeled as 1 (i.e., suitable for QRL). The validation set consisted of 2126 visual representations labeled as 0 and 1258 representations labeled as 1.

The training and validation representations were labeled

OMP Configuration	Memory Representation	tAP <sub>25</sub> ↑	stAP <sub>25</sub> ↑	Succ ↑	Size ↓
OD <sub>oracle</sub> OT <sub>oracle</sub>	MR1*	0.73	0.68	81.92	7.1 MB
	MR2	0.73	0.68	81.92	395 MB
	MR3	0.63	0.55	74.33	<b>2.6 MB</b>
	MR4	<b>0.79</b>	<b>0.71</b>	<b>83.38</b>	38.5 MB
OD <sub>yolo</sub> OT <sub>oracle</sub>	MR1*	0.21	<b>0.19</b>	40.55	11.2 MB
	MR2	0.21	<b>0.19</b>	40.55	94.0 MB
	MR3	0.20	0.17	38.02	<b>1.0 MB</b>
	MR4	<b>0.22</b>	<b>0.19</b>	<b>41.82</b>	100.8 MB
OD <sub>oracle</sub> OT <sub>egostark</sub>	MR1*	<b>0.18</b>	<b>0.05</b>	<b>31.91</b>	40.3 MB
	MR2	<b>0.18</b>	<b>0.05</b>	<b>31.91</b>	350.0 MB
	MR3	0.16	0.03	26.56	<b>3.1 MB</b>
	MR4	0.16	0.04	29.02	4.1 GB
OD <sub>yolo</sub> OT <sub>egostark</sub>	MR1*	<b>0.0003</b>	<b>0.002</b>	<b>4.02</b>	209.3 MB
	MR2	<b>0.0003</b>	<b>0.002</b>	<b>4.02</b>	2.3 GB
	MR3	0.0002	0.0003	1.78	<b>105.1 MB</b>
	MR4	0.0002	0.0005	2.90	746.6 MB

Table 6. **Effect of memory representation in ESOM.** This table illustrates the impact of using different representations for  $\mathcal{M}_{ego}$  on QRL performance and memory size. MR1\* refers to the representation described in the main paper. As can be noticed, MR1\* constitutes the best approach at the intersection of QRL accuracy and memory efficiency. (Best results are highlighted in **bold**).

as 0 or 1 based on whether they were incorrectly or correctly matched by the QRL algorithm. For each frame in the 250 selected clips, the representation  $\phi_i$  of the annotated visual query  $\mathbf{Q}_i$  was extracted, and its feature representation  $\Phi(\phi_i)$  was computed using DINOv2 [30] as  $\Phi(\cdot)$ . This representation was then compared to  $\Phi(\phi_{i,t})$ , the feature representation of the patches within the ground-truth bounding-boxes of the tracklet associated with the query  $\mathbf{Q}_i$ , using cosine similarity. This comparison produced a similarity score  $s_t$  ranging from 0 to 1. Patches were assigned negative labels if  $s_t \leq 0.3$  and positive labels if  $s_t \geq 0.7$ . After labeling, the data was randomly split into training and validation sets, with 80% allocated to the training set and 20% to the validation set.

The visual representation classifier was fine-tuned for 50 epochs using Stochastic Gradient Descent (SGD) with a learning rate of 0.01. At convergence, it achieved a test accuracy of 96%. The input patches were resized to  $224 \times 224$  pixels before being fed into the model.

## A.2. Object Memory Population (OMP)

### A.2.1 Object Tracking (OT) module.

In this section, we provide details regarding the implementation of OT module. In Table 7, we report the performance of the different implementations as measured by standard multiple object tracking (MOT) metrics [28].

**OT<sub>egostark</sub>.** OT<sub>egostark</sub> implements a multiple-object tracking approach using multiple instances of single-object trackers. This approach is motivated by the lack of effective multiple-object tracking solutions for egocentric vision, whereas single-object tracking has been extensively studied [9, 10, 42]. For single-object tracking, we use the STARK framework [48], fine-tuned on the EgoTracks dataset as de-

Tracker	Detector	HOTA ↑	OWTA ↑	AssA ↑	LocA ↑
MASA	GroundingDino	0.036	<b>0.211</b>	0.105	0.766
MASA	YOLOv10*	<b>0.066</b>	0.080	0.116	0.798
MASA	Ground-truth	0.501	0.501	0.252	1.000
EgoSTARK	Hand-Object Detector	0.034	0.121	0.102	0.739
EgoSTARK	GroundingDino	0.057	0.121	0.115	<b>0.803</b>
EgoSTARK	YOLOv10*	0.061	0.188	<b>0.151</b>	0.801
EgoSTARK	Ground-truth	0.217	0.390	0.347	0.831
Ground-truth	YOLOv10*	0.848	0.848	0.943	1.000
Ground-truth	GroundingDino	0.875	0.875	0.943	1.000

Table 7. **Evaluation of different tracking algorithms for the implementation of the Object Tracking (OT) module.** We evaluated the multi-object tracking (MOT) performance of our implementations on EgoTracks’s validation set. Models marked with “\*” are finetuned on EgoTracks [42]. Ground-truth refers to the EgoTracks annotations used to simulate optimal object detection or tracking, and the respective results are reported in gray. We found the AssA results to be best indicators for QRL accuracy. (Best results, across real-world tracker-detector combinations, are highlighted in **bold**.)

scribed in [42], resulting in the EgoSTARK tracker. To track multiple objects, we instantiate multiple EgoSTARK trackers simultaneously. A new tracker instance is initialized in frame  $\mathbf{F}_t$  whenever the OD module identifies a valid object, which is then stored in memory. Each bounding-box predicted by the OD module serves as a template to initialize a corresponding tracker. Once initialized, a tracker runs across subsequent frames to predict the bounding boxes of the object it was assigned to, thereby updating the spatiotemporal representation of the respective object. Due to the challenges of object tracking in egocentric vision [9, 10, 42], we found different tracker instances to often end in tracking the same object. In order to prevent duplicate tracker instances, we calculate the IoU between all tracked objects at frame  $t$ . If two tracking predictions overlap with an IoU greater than 0.5, the trackers are considered to be duplicate trackers and only the tracker instance and their corresponding prediction with the lower object instance ID (i.e. the older object) is kept.

Furthermore, to prevent incorrect tracking predictions from causing a tracker to deviate from a searching area that contains the target object and wander across the frame, the box used to compute the search region for the subsequent frame is not updated if the confidence score of the EgoSTARK instance falls below 0.4. This strategy is based on the observation that, in egocentric vision, objects often leave the frame during rapid head movements but typically reappear in a similar location when the head returns to its original position. Before writing the OT module predictions to  $\mathcal{M}_{ego}$ , the bounding-boxes  $\mathbf{b}_{i,t}$  with confidence score  $s_{i,t} > \lambda_{ot} = 0.5$  are retained.

**OT<sub>masa</sub>.** As an alternative approach, we implemented the state-of-the-art association method MASA [23] as a multi-object tracker, utilizing object detections provided by the



Figure 7. **Visualization of discarded bounding-boxes.** Small-area bounding-boxes similar to those shown in this figure have been discarded for the training and evaluation of the module. This is because we found that they lacked sufficient visual information, leading to an increased number of false positive detections. These detections provided no useful data for tracker initialization within the OT module or for effective QRL.

OD module. We set a score threshold of 0.1 and limited object comparisons to the last ten frames using the MASA adapter. To evaluate the impact of considering more frames, we tested with 150 previous frames, but this led to a drop in the OWTA metric from 0.2111 to 0.1496. This result highlights the challenges the MASA adapter faces with long-term tracking.

## A.2.2 Object Discovery (OD) module

**Clustering-based object taxonomy on EgoTracks.** As detecting objects from egocentric videos is not straightforward [51], we tested different object detectors including the off-the-shelf detectors GroundingDino [26] and the hand-object detector of [39] (here referred to as Hand-Object Detector) which do not require training on the considered settings, as well as Faster R-CNN R101-FPN [36] and YOLOv10 [45] instances trained on different data sources, including EgoObjects [51] and curated versions of EgoTracks [42]. Targeting visual object tracking, EgoTracks contains spatially-sparse bounding box annotations across contiguous frames (i.e., only few object instances are annotated in each frame). Each object instance is associated to a textual description rather than an object class (e.g., “a blue bottle”). To enable the training of object detectors, we first clustered object descriptions with K-Means to obtain an initial set of 1169 classes, followed by manual refinement in order to adjust them, leading to a diverse, granular taxonomy comprising 295 classes.

**Data cleaning for EgoTracks.** Since EgoTracks contains annotations in contiguous frames, we uniformly sampled one third of all frames. EgoTracks contains annotations for very small objects to assess the ability of visual object trackers to continuously follow objects subject to scale changes.

Since these objects would be unfeasible to detect from single frames and may be source of ambiguity due to occlusion or motion blur, we discarded bounding box annotations with areas falling in the first quartile of all bounding box areas in the training set. Figure 7 shows a few examples of annotation bounding boxes that fall in the first quartile and therefore discarded from the dataset. This leads to a reduced training set of 474,761 annotated images, while we consider a validation set of 2,466 images.

**Faster R-CNN - based detector.** A first version of the object discovery module is obtained by training a Faster R-CNN instance on the above described dataset with object class taxonomies obtained through clustering of object descriptions. The performance of this module is limited as shown later in the quantitative evaluation, so this implementation of the OD module is not considered in the main paper.

**YOLOv10 - based detector.** A second version of the object discovery module was based on the YOLOv10 [45] object detector, given its capacity for real-time inference. We trained the YOLO detector on the same set of refined EgoTracks annotations. Given the sparsity of EgoTracks annotations, both the Faster R-CNN and YOLO detectors tend to recognize few object instances per image, which may limit the ability of the object discovery module to identify all possible objects of interest. To address this issue, we trained the YOLO object detector on the EgoObjects [51] dataset, which contains dense object annotations for egocentric frames with a fixed taxonomy of 638 classes. To make the EgoObjects and EgoTracks sets compatible, we mapped each EgoTracks object description to its corresponding class from the EgoObjects taxonomy. This is done by first describing the object description and class name with a *Sentence Transformer*, and then selecting the class maximizing the cosine similarity between the embeddings. To reduce noise, we discarded all annotations with a similarity lower than 0.7.

**Examples of class mapping.** Table 8 shows some examples of object descriptions retrieved from the EgoTracks annotations and mapped to EgoObjects objects. Note that some objects such as “air conditioner”, “headphones” or “yoga mat” have a reasonable match, while “washing machine” contains “flat washer”, which has a different meaning despite a close embedding. We did not manually adjust these inconsistencies to keep the process fully automated. The table contains one class with no matches (accordion), due to the absence of EgoTracks objects with similar descriptions. Out of the total number of class descriptions (3491), we mapped 1241 captions, while the remaining 2250 classes were excluded from the dataset. This resulted in a high-quality subset of the data suitable for training and evaluation.

**Quantitative comparison.** Despite the domain difference between EgoObjects and EgoTracks, we noticed improved



EgoObjects Classes	accordion	air conditioner	headphones	washing machine	...	yoga mat
EgoTracks Mapped Classes	-	air conditioner, air conditioner control, air conditioner., air conditioning machine	head phones, headphone, headphones, headset, earphone, earphones	flat washer, washing machine	...	gym mat, mat, workout mat, yoga mat, exercise mat, fitness mat

Table 8. **Examples of class mappings from EgoObject classes to EgoTracks object descriptions.** The first row reports EgoObject classes, while the second row contains descriptions of EgoTracks matched with embedding similarity.

qualitative and quantitative results. To further adapt the model to the EgoTracks domain, we fine-tuned the YOLO object detector, pre-trained on EgoObjects, on the EgoTracks dataset with labels mapped to the EgoObjects taxonomy. Table 9 compares the performance of the considered approaches with two off-the-shelf object detectors: GroundingDino [26] and the Hand-Object-Detector of [39]. We do not train these detectors on the EgoTracks data and use the official checkpoints and implementations provided by the authors. Since Visual Query Localization does not require to correctly identify object classes, all methods are evaluated with AP and Recall, merging all ground truth and predicted classes in a single “object” class. It is worth noting that AP and Recall measure different aspects of the detector. Indeed, AP measures the average ratio between correct predictions and all predictions made by the detector, whereas Recall measures the fraction of objects which have been correctly found by the detector, regardless of the total number of objects. In our settings, it is desirable to have a large recall (future queries have more chance to end up in the memory), but, since it is not possible to track all objects and a select must be made based on the confidence score, in practice, a very low value of AP is not desirable. The harmonic mean between AP and Recall is hence adopted as a way to identify the most balanced detector. Results in Table 9, obtained with a confidence score threshold  $\lambda_{od} = 0.01$ , show that Faster R-CNN trained on labels clustered from EgoTracks achieves the highest recall (0.5224), but also yields a very low AP value (0.0219). On the contrary, the YOLO instance achieves the highest AP (0.1983) but also a low recall (0.1634). We attribute these skewed results to the sparse nature of annotations in EgoTracks (only few object instances annotated per frame) and the different ways of the two methods to handle negative examples. The harmonic mean results of the first one are rather low (0.0420), while the second result is higher but not optimal at 0.1791, highlighting the unbalanced nature of the two approaches. Training YOLO on EgoObjects, which contains much denser annotations increases Recall to 0.3780 at the expense of AP (0.0247), which leads to a low harmonic mean of 0.0463. Mapping EgoTracks annotations to the EgoObjects taxonomy and training YOLO using both datasets provides the most balanced detector, with an

harmonic mean of 0.1882, an AP of 0.1358 and a Recall of 0.3067. GroundingDino achieves a low AP and a reasonable recall value (0.0450 and 0.2572), which is likely due to the large domain shift between data used for training GroundingDino and the challenging egocentric observations of EgoTracks. Using Hand-Object-Detector as an object detector leads to lower results, which is due to the fact that the Hand-Object-Detector only focuses on interacted objects, hence neglecting many non-interacted objects which may nevertheless be queried in the future. Lastly, RT-DETR (used in VideoAgent [11]) achieves results comparable to GroundingDino, due to similar reasons.

**Qualitative Examples.** Figure 8 reports qualitative examples, reporting the predictions of the discussed models on a frame from the validation set of EgoTracks. Results are consistent with the evaluation metrics in Table 9, Faster R-CNN (A) is the model with the highest recall, indeed it is the model with the highest number of bounding boxes containing both correctly localized objects and errors. YOLO trained on EgoTracks (B) has fewer predictions than Faster R-CNN, but they are more accurate. Training YOLO on EgoTracks (C) shows similar results to Faster R-CNN, with the second densest predictions, translated into the second-highest recall model. YOLO trained on EgoObjects fine-tuned in EgoTracks (D) has the most balanced results; predictions are well localized, reflecting the best performing model in the HM metric. GroundingDino (E) contains several correctly regressed objects, but as shown in the frame, no ground truth annotations were found. Hand-Object-Detector (F) has the worst performance, containing only two predictions, one of which is related to the interacted object. The discovery mechanism of this detector leads to the lowest values for both precision and recall. The predictions of VideoAgent (G) are partially correct, despite the presence of a few wrong bounding boxes. Finally the predictions marked with H are the ground truth ones.

**OD<sub>yolo</sub> and OD<sub>gdino</sub>.** Given these results, in the following experiments, we consider the YOLO detector trained on EgoObjects and EgoTracks as a representative of trained methods and both GroundingDino and Hand-Object-Detector as representative of off-the-shelf methods. These are referred to as OD<sub>yolo</sub> and OD<sub>gdino</sub> respectively in the main paper.

Detector	Training Dataset	AP $\uparrow$	Rec $\uparrow$	HM $\uparrow$
Faster R-CNN	EgoTracks*	0.0219	<b>0.5224</b>	0.0420
YOLO	EgoTracks*	<b>0.1983</b>	0.1634	0.1791
YOLO	EgoObjects	0.0247	0.3780	0.0463
YOLO	EgoObjects + EgoTracks**	0.1358	0.3067	<b>0.1882</b>
GroundingDino	-	0.0450	0.2572	0.0765
Hand-Object Detector	-	0.0247	0.0381	0.0299
RT-DETR	-	0.0418	0.3374	0.0743

Table 9. **Comparison of the different object detectors.** \* denotes that the object taxonomy has been obtained through clustering. \*\* denotes that classes have been obtained by mapping EgoTracks descriptions to the EgoObject taxonomy. HM: Harmonic Mean between AP and Recall. (Best results are highlighted in **bold**.)



Figure 8. **Visualization of predictions from the object detection models.** Here we qualitatively show the performance of the different object detectors over the same sampled frame. A: Faster R-CNN on EgoTracks, B: YOLO on EgoTracks, C: YOLO on EgoObjects, D: YOLO on EgoObjects, fine-tuned in EgoTracks, E: GroundingDino, F: is the Hand-Object Detector G: RT-DETR, H: Ground-truth annotations.

### A.3. Query Retrieval and Localization (QRL)

We implemented two distinct approaches for localizing a visual query  $\mathbf{Q}$  within a memory  $\mathcal{M}_{ego}$ : an implementation based on SiamRCNN with a classification head [44] ( $QRL_{siamrcnn}$ ); and an approach based on DINOv2 with cosine similarity [17, 30] ( $QRL_{dino}$ ).

In  $QRL_{siamrcnn}$ , a Feature Pyramid Network (FPN) [24] serves as the backbone  $\Phi(\cdot)$  for features extraction, generating features for the visual representation of the object

$\Phi(\phi_{i,t}), \phi_{i,t} \neq \emptyset$  stored in  $\mathcal{M}_{ego}$  as well as the features for the visual query  $\Phi(\mathbf{Q})$ . To determine whether  $\mathbf{Q}$  exists within  $\mathcal{M}_{ego}$ , each  $\Phi(\phi_{i,t})$  is compared with  $\Phi(\mathbf{Q})$  using a siamese network head,  $\Psi(\Phi(\phi_{i,t}), \Phi(\mathbf{Q}))$ , which implements a bilinear operation [44] that predicts instance similarity score belonging to the interval  $[0, 1]$ .

In  $QRL_{dino}$ , DINOv2 [30] is employed as the backbone  $\Phi(\cdot)$  for extracting feature representations  $\Phi(\phi_{i,t})$  and  $\Phi(\mathbf{Q})$ . In this approach, the similarity operation  $\Psi(\Phi(\phi_{i,t}), \Phi(\mathbf{Q}))$  is implemented using cosine similarity [17], which provides scores belonging to the interval  $[0, 1]$ .

In both cases, for each object  $i$ , the similarity scores are averaged into a single score  $r_i$ . If the maximum score  $r_i$  exceeds the threshold  $\lambda_{ref} = 0.5$ , the object  $\mathbf{O}_i$  is considered a match for query  $\mathbf{Q}$ . Once match is identified, the most recent sequence of contiguous bounding-boxes from  $\mathbf{O}_i$ 's spatio-temporal history is retrieved and returned as the response track  $\mathbf{r}$ .

## B. Online Object Memory Baselines

Here we provide details of the implementations of the baselines used for comparison in Table 2.

### B.1. AMEGO

The AMEGO framework [17], was employed to construct an episodic memory model, serving as a performance benchmark for our proposed approach. We utilized *ce683bd* version of the AMEGO codebase, available at <sup>6</sup>, with minor modifications to accommodate the EGO4D dataset structure. Our implementation focused specifically on the Hand-Object Interaction (HOI) module of AMEGO. The Location Segmentation module was excluded from our analysis as it fell outside the scope of our research objectives. To ensure a fair and consistent comparison, we maintained the original hyperparameters and thresholds to align with the baseline model published on the official GitHub repository. Since their experiment has been made using a different dataset, our modifications were limited to data input/output functions to handle the EGO4D data format, without altering the core algorithmic components.

### B.2. VideoAgent

The VideoAgent framework [11], has been utilized as a comparative baseline for our episodic memory model. We employed the *21e4eb7* version of the VideoAgent repository<sup>7</sup>. Our implementation focused on the Object Memory module, and we opted to omit the captioning module since it was not pertinent to our research scope. To maintain experimental integrity, we preserved the original configuration

<sup>6</sup><https://github.com/gabrielegoletto/AMEGO.git>

<sup>7</sup><https://github.com/YueFan1014/VideoAgent.git>

parameters.

### B.3. Memory Representation

As with the other OMP configurations discussed in this paper, the object tracklets produced by VideoAgent and Amego OMP are stored in memory using the MR1\* representation, as it provides the best balance between accuracy and memory efficiency (see Table 6). Specifically, for each  $\mathbf{O}_i$  found by either AMEGO or VideoAgent object detection and tracking algorithms,  $\mathcal{M}_{ego}$  retains the RGB patch ( $\phi_{i,t}$ ) and the  $\mathbf{b}_{i,t}$  at the time of object discovery, along with two RGB patches from the most recent response track. These patches correspond to the first and last valid patches identified by the classifier within the most recent sequence of bounding-boxes. For all other temporal locations not covered above,  $\mathcal{M}_{ego}$  stores only the spatio-temporal information provided by  $\mathbf{b}_{i,t}$ .

### B.4. Query Retrieval and Localization (QRL)

To localize the visual queries  $\mathbf{Q}$  within the memory  $\mathcal{M}_{ego}$  built over AMEGO and VideoAgent, we used the implementation based on SiamRCNN with a classification head (QRL<sub>siamrcnn</sub>). Once the similarity scores are computed for the different patches, they are averaged into a single score  $r_i$ . If the maximum score exceeds the  $\lambda_{ret} = 0.5$ , the object  $\mathbf{O}_i$  is considered a match for query  $\mathbf{Q}$ .

## C. Evaluation Dataset

Due to the high storage requirements for the validation split of the Ego4D VQ2D benchmark [18] and the significant time needed for experiments on the full dataset, we opted to use a subset of the validation clips for our evaluations. Specifically, we randomly selected 115 video clips uniformly, containing 450 visual queries along with their corresponding ground-truth response tracks and tracklets. This subset consisted of a total of 208365 frames. To maintain consistency with the original frame rate of the EGO4D dataset [18], we ran the OMP algorithm at 5 frames per second.

## D. Additional Results

**Combination of OD modules.** The performance of ESOM has been evaluated under various configurations of the OD and OT modules (Table 5). However, OMP configurations using  $\text{OD}_{oracle}$  construct a memory that includes only objects that will be queried. To incorporate additional legitimate objects into  $\mathcal{M}_{ego}$ , we combined the oracle detections, together with the  $\text{OD}_{yolo}$  detections (see  $\text{OD}_{oracle+yolo}$  in Table 10). Adding more objects to memory reduces ESOM’s performance compared to the OMP configuration with  $\text{OD}_{oracle}$ . This suggests that an increased number of objects in memory hinders the QRL al-

OMP Configuration		tAP <sub>25</sub> ↑	stAP <sub>25</sub> ↑	Succ ↑	Size ↓
OD	OT				
$\text{OD}_{oracle}$	$\text{OT}_{egostark}$	<b>0.18</b>	<b>0.05</b>	<b>31.91</b>	<b>40.3 MB</b>
$\text{OD}_{yolo}$	$\text{OT}_{egostark}$	0.0003	0.002	4.02	209.3 MB
$\text{OD}_{oracle+yolo}$	$\text{OT}_{egostark}$	0.10	0.02	23.67	229.4 MB

Table 10. **More objects in the memory can confound QRL.** In this table, by combining the capabilities of the  $\text{OD}_{oracle}$  and  $\text{OD}_{yolo}$ , we tested whether the QRL method is robust to a memory  $\mathcal{M}_{ego}$  which contains the true visual queries as well as other object found while processing  $\mathcal{V}_{ego}$ . (Best results are in **bold**).

gorithm’s ability to accurately discriminate the visual query, resulting in confusion. However, its performance remains higher than the OMP configuration using only  $\text{OD}_{yolo}$ , further highlighting the challenges detectors face in identifying objects that will appear as queries in the future.

**Qualitative examples.** Figure 9 shows additional qualitative examples of the behavior of QRL in retrieving and localizing different visual queries within two memory representations build by two OMP configurations.

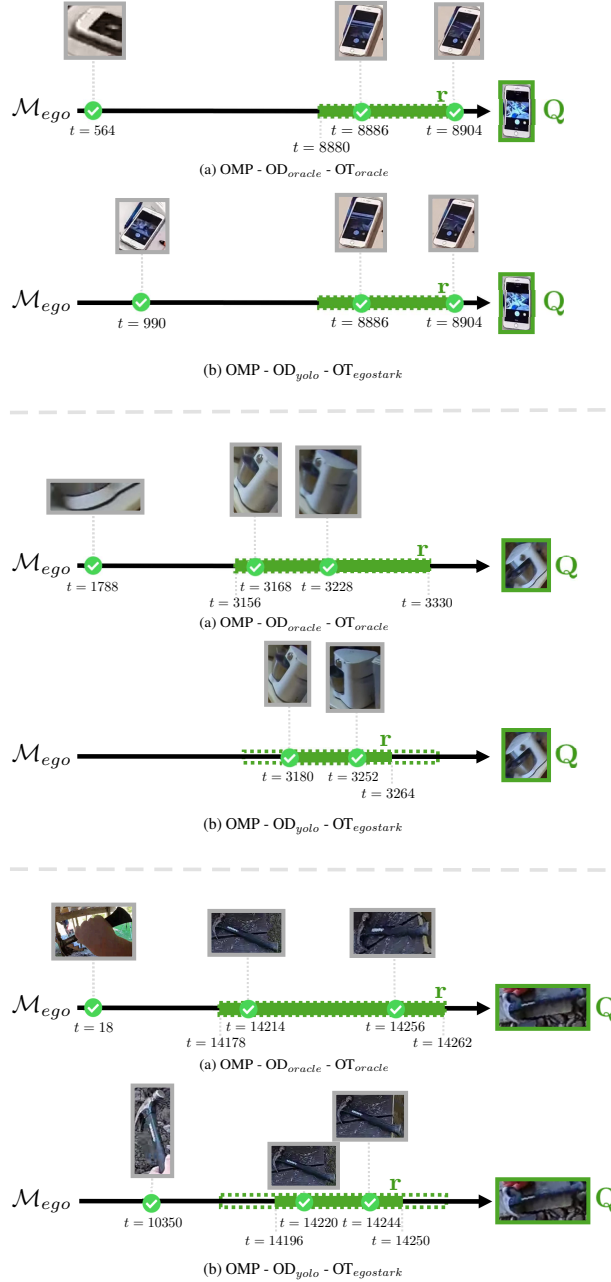


Figure 9. **Additional qualitative examples.** Successful retrievals of three different queries  $Q$  from  $\mathcal{M}_{ego}$  are shown using (a) the oracle OMP algorithm ( $OD_{oracle} - OT_{oracle}$ ) and (b) the real-world OMP ( $OD_{yolo} - OT_{egostark}$ ). The figure highlights the visual representations stored in  $\mathcal{M}_{ego}$  and matched during retrieval, their respective timestamps, the duration of the response track  $r$  returned by QRL, and the extent of the ground-truth response track (the rectangle with dashed outline).

## References

- [1] Joungbin An, Hyolim Kang, Su Ho Han, Ming-Hsuan Yang, and Seon Joo Kim. Miniroad: Minimal rnn framework for online action detection. In *ICCV*, 2023. 3
- [2] Leonard Bärmann and Alex Waibel. Where did i leave my keys?-episodic-memory-based question answering on egocentric videos. In *CVPRW*, 2022. 3
- [3] Gedas Bertasius, Heng Wang, and Lorenzo Torresani. Is space-time attention all you need for video understanding? In *ICML*, 2021. 3
- [4] Goutam Bhat, Martin Danelljan, Luc Van Gool, and Radu Timofte. Know your surroundings: Exploiting



- scene information for object tracking. In *ECCV*, 2020. 3
- [5] João Carreira and Andrew Zisserman. Quo vadis, action recognition? a new model and the kinetics dataset. In *CVPR*, 2017. 3
- [6] Guo Chen, Sen Xing, Zhe Chen, Yi Wang, Kunchang Li, Yizhuo Li, Yi Liu, Jiahao Wang, Yin-Dong Zheng, Bingkun Huang, et al. Internvideo-ego4d: A pack of champion solutions to ego4d challenges. *arXiv preprint arXiv:2211.09529*, 2022. 2, 3
- [7] Dima Damen, Hazel Doughty, Giovanni Maria Farinella, Antonino Furnari, Evangelos Kazakos, Jian Ma, Davide Moltisanti, Jonathan Munro, Toby Perrett, Will Price, and Michael Wray. Rescaling egocentric vision: Collection, pipeline and challenges for epic-kitchens-100. *IJCV*, 2022. 3
- [8] Roeland De Geest, Efstratios Gavves, Amir Ghodrati, Zhenyang Li, Cees Snoek, and Tinne Tuytelaars. Online action detection. In *ECCV*. Springer, 2016. 3
- [9] Matteo Dunnhofer, Antonino Furnari, Giovanni Maria Farinella, and Christian Micheloni. Is first person vision challenging for object tracking? In *ICCVW*, 2021. 6, 2
- [10] Matteo Dunnhofer, Antonino Furnari, Giovanni Maria Farinella, and Christian Micheloni. Visual object tracking in first person vision. *IJCV*, 2023. 6, 2
- [11] Yue Fan, Xiaojian Ma, Rujie Wu, Yuntao Du, Jiaqi Li, Zhi Gao, and Qing Li. Videoagent: A memory-augmented multimodal agent for video understanding. In *ECCV*, 2024. 3, 6, 7, 1, 4, 5
- [12] Christoph Feichtenhofer, Haoqi Fan, Jitendra Malik, and Kaiming He. Slowfast networks for video recognition. In *ICCV*, 2019. 3
- [13] Yisen Feng, Haoyu Zhang, Yuquan Xie, Zaijing Li, Meng Liu, and Liqiang Nie. Objectnlq@ ego4d episodic memory challenge 2024. *arXiv preprint arXiv:2406.15778*, 2024. 2
- [14] Antonino Furnari and Giovanni Farinella. Rolling-unrolling lstms for action anticipation from first-person video. *IEEE TPAMI*, 2021. 3
- [15] Jiyang Gao, Zhenheng Yang, and Ram Nevatia. RED: Reinforced encoder-decoder networks for action anticipation. In *BMVC*, 2017.
- [16] Rohit Girdhar and Kristen Grauman. Anticipative video transformer. In *ICCV*, 2021. 3
- [17] Gabriele Goletto, Tushar Nagarajan, Giuseppe Averta, and Dima Damen. Amego: Active memory from long egocentric videos. In *ECCV*, 2024. 3, 5, 6, 7, 1
- [18] Kristen Grauman et al. Ego4d: Around the World in 3,000 Hours of Egocentric Video. In *CVPR*, 2022. 2, 3, 5, 6, 1
- [19] Kaiming He, Xiangyu Zhang, Shaoqing Ren, and Jian Sun. Deep residual learning for image recognition. In *CVPR*, 2016. 1
- [20] Minh Hoai and Fernando De la Torre. Max-margin early event detectors. *IJCV*, 2014. 3
- [21] Yixuan Huang, Jialin Yuan, Chanho Kim, Pupul Pradhan, Bryan Chen, Li Fuxin, and Tucker Hermans. Out of sight, still in mind: Reasoning and planning about unobserved objects with video tracking enabled memory models. *arXiv preprint arXiv:2309.15278*, 2023. 3
- [22] Hanwen Jiang, Santhosh Kumar Ramakrishnan, and Kristen Grauman. Single-stage visual query localization in egocentric videos. In *NeurIPS*, 2023. 2, 3, 6
- [23] Siyuan Li, Lei Ke, Martin Danelljan, Luigi Piccinelli, Mattia Segu, Luc Van Gool, and Fisher Yu. Matching anything by segmenting anything. In *CVPR*, 2024. 5, 2
- [24] Tsung-Yi Lin, Piotr Dollár, Ross Girshick, Kaiming He, Bharath Hariharan, and Serge Belongie. Feature pyramid networks for object detection. In *CVPR*, 2017. 5
- [25] Naiyuan Liu, Xiaohan Wang, Xiaobo Li, Yi Yang, and Yueting Zhuang. Reler@ zju-alibaba submission to the ego4d natural language queries challenge 2022. *arXiv preprint arXiv:2207.00383*, 2022. 2
- [26] Shilong Liu, Zhaoyang Zeng, Tianhe Ren, Feng Li, Hao Zhang, Jie Yang, Qing Jiang, Chunyu Ren, Jianwei Yang, Hang Su, et al. Grounding dino: Marrying dino with grounded pre-training for open-set object detection. *arXiv preprint arXiv:2303.05499*, 2023. 5, 3, 4
- [27] Shuming Liu, Chen-Lin Zhang, Chen Zhao, and Bernard Ghanem. End-to-end temporal action detection with 1b parameters across 1000 frames. In *CVPR*, 2024. 3
- [28] Jonathon Luiten, Aljosa Osep, Patrick Dendorfer, Philip Torr, Andreas Geiger, Laura Leal-Taixé, and Bastian Leibe. Hota: A higher order metric for evaluating multi-object tracking. *IJCV*, 2021. 7, 2
- [29] Jinjie Mai, Abdullah Hamdi, Silvio Giancola, Chen Zhao, and Bernard Ghanem. EgoLoc: Revisiting 3d object localization from egocentric videos with visual queries. In *ICCV*, 2023. 2
- [30] Maxime Oquab, Timothée Darcet, Théo Moutakanni, Huy Vo, Marc Szafraniec, Vasil Khalidov, Pierre Fernandez, Daniel Haziza, Francisco Massa, Alaaeldin El-Nouby, et al. Dinov2: Learning robust visual features without supervision. *arXiv preprint arXiv:2304.07193*, 2023. 5, 2
- [31] Baoqi Pei, Guo Chen, Jilan Xu, Yuping He, Yicheng Liu, Kanghua Pan, Yifei Huang, Yali Wang, Tong Lu, Limin Wang, et al. EgoVideo: Exploring egocentric

- foundation model and downstream adaptation. *arXiv preprint arXiv:2406.18070*, 2024. 2, 3
- [32] Chiara Plizzari, Shubham Goel, Toby Perrett, Jacob Chalk, Angjoo Kanazawa, and Dima Damen. Spatial cognition from egocentric video: Out of sight, not out of mind. *arXiv preprint arXiv:2404.05072*, 2024. 3
- [33] Chiara Plizzari, Gabriele Goletto, Antonino Furnari, Siddhant Bansal, Francesco Ragusa, Giovanni Maria Farinella, Dima Damen, and Tatiana Tommasi. An outlook into the future of egocentric vision. *IJCV*, 2024. 2
- [34] Santhosh Kumar Ramakrishnan, Ziad Al-Halah, and Kristen Grauman. Naq: Leveraging narrations as queries to supervise episodic memory. In *CVPR*, 2023. 2
- [35] Santhosh Kumar Ramakrishnan, Ziad Al-Halah, and Kristen Grauman. Spotem: efficient video search for episodic memory. In *ICML*, 2023. 2
- [36] Shaoqing Ren, Kaiming He, Ross Girshick, and Jian Sun. Faster r-cnn: Towards real-time object detection with region proposal networks. *IEEE TPAMI*, 2016. 3
- [37] Ivan Rodin, Antonino Furnari, Dimitrios Mavroedis, and Giovanni Maria Farinella. Predicting the future from first person (egocentric) vision: A survey. 2021. 3
- [38] Mohammad Sadegh Aliakbarian, Fatemeh Sadat Saleh, Mathieu Salzmann, Basura Fernando, Lars Petersson, and Lars Andersson. Encouraging lstms to anticipate actions very early. In *ICCV*, 2017. 3
- [39] Dandan Shan, Jiaqi Geng, Michelle Shu, and David F Fouhey. Understanding human hands in contact at internet scale. In *CVPR*, 2020. 3, 4
- [40] Kiran Somasundaram, Jing Dong, Huixuan Tang, Julian Straub, Mingfei Yan, Michael Goesele, Jakob Julian Engel, Renzo De Nardi, and Richard Newcombe. Project aria: A new tool for egocentric multi-modal ai research. *arXiv preprint arXiv:2308.13561*, 2023. 2
- [41] Alexandros Stergiou and Dima Damen. The wisdom of crowds: Temporal progressive attention for early action prediction. In *CVPR*, 2023. 3
- [42] Hao Tang, Kevin J Liang, Kristen Grauman, Matt Feiszli, and Weiyao Wang. Egotracks: a long-term egocentric visual object tracking dataset. In *NeurIPS*, 2023. 5, 6, 7, 1, 2, 3
- [43] Endel Tulving. Episodic memory: From mind to brain. *Annual review of Psychology*, 2002. 2
- [44] Paul Voigtlaender, Jonathon Luiten, Philip HS Torr, and Bastian Leibe. Siam r-cnn: Visual tracking by re-detection. In *CVPR*, 2020. 2, 5, 6
- [45] A Wang, H Chen, L Liu, K Chen, Z Lin, J Han, and G Ding. Yolov10: Real-time end-to-end object detection. arxiv 2024. *arXiv preprint arXiv:2405.14458*. 5, 3
- [46] Mengmeng Xu, Cheng-Yang Fu, Yanghao Li, Bernard Ghanem, Juan-Manuel Perez-Rua, and Tao Xiang. Negative frames matter in egocentric visual query 2d localization, 2022. 2, 3
- [47] Mengmeng Xu, Yanghao Li, Cheng-Yang Fu, Bernard Ghanem, Tao Xiang, and Juan-Manuel Pérez-Rúa. Where is my wallet? modeling object proposal sets for egocentric visual query localization. In *CVPR*, 2023. 2, 3, 6
- [48] Bin Yan, Houwen Peng, Jianlong Fu, Dong Wang, and Huchuan Lu. Learning spatio-temporal transformer for visual tracking. In *ICCV*, 2021. 5, 6, 2
- [49] Chen-Lin Zhang, Jianxin Wu, and Yin Li. Action-former: Localizing moments of actions with transformers. In *ECCV*. Springer, 2022. 3
- [50] Yue Zhao and Philipp Krähenbühl. Real-time online video detection with temporal smoothing transformers. In *ECCV*, 2022. 3
- [51] Chenchen Zhu, Fanyi Xiao, Andrés Alvarado, Yasmine Babaei, Jiabo Hu, Hichem El-Mohri, Sean Culatana, Roshan Sumbaly, and Zhicheng Yan. Egoobjects: A large-scale egocentric dataset for fine-grained object understanding. In *ICCV*, 2023. 5, 6, 7, 3